

Topological Mapping for Manhattan-like Repetitive Environments

Sai Shubodh Puligilla*, Satyajit Tourani*, Tushar Vaidya*, Udit Singh Parihar*,
Ravi Kiran Sarvadevabhatla and K. Madhava Krishna

Abstract—We showcase a topological mapping framework for a challenging indoor warehouse setting. At the most abstract level, the warehouse is represented as a Topological Graph where the nodes of the graph represent a particular warehouse topological construct (e.g. rackspace, corridor) and the edges denote the existence of a path between two neighbouring nodes or topologies. At the intermediate level, the map is represented as a Manhattan Graph where the nodes and edges are characterized by Manhattan properties and as a Pose Graph at the lower-most level of detail. The topological constructs are learned via a Deep Convolutional Network while the relational properties between topological instances are learnt via a Siamese-style Neural Network. In the paper, we show that maintaining abstractions such as Topological Graph and Manhattan Graph help in recovering an accurate Pose Graph starting from a highly erroneous and unoptimized Pose Graph. We show how this is achieved by embedding topological and Manhattan relations as well as Manhattan Graph aided loop closure relations as constraints in the backend Pose Graph optimization framework. The recovery of near ground-truth Pose Graph on real-world indoor warehouse scenes vindicate the efficacy of the proposed framework.

I. INTRODUCTION

This paper explores the role of topological understanding and the concomitant benefits of such an understanding to the SLAM framework. Figure-1 shows an erroneous Pose Graph (PG) labelled ‘a’, while the topological graph TG is shown labelled as ‘b’ in the same figure succinctly. Each node in the TG is labelled by the Deep Convolutional Network. The TG is converted to a Manhattan Graph (MG) wherein the Manhattan properties of the nodes (length or width of the topology) and edges are gleaned from the PG . While the MG facilitate seamless loop detection between a pair of Manhattan nodes, such relations when integrated with a backend SLAM framework, enables recovery of an optimized pose-graph and corresponding map. The crux of the paper lies in detailing the framework and its efficacy in challenging real world settings of two different warehouses.

There have been a number of works in this area and a detailed review of such methods can be seen in [1]. Prominent and well cited amongst these include [2], [3], [4], [5], [6]. Most of these methods are focused exclusively on vision based loop detection with invariant descriptors. Many relate to an individual image as a distinct topology of the scene without relating such nodes to a meta-level label such as a rackspace, corridor, intersection etc. Some seminal works as [7] show recovery from wrong loop closures in a Manhattan

environment though they don’t discuss how the original MG is constructed and how such relations can be integrated into a backend SLAM. [8] shows how a Bayesian inference over topologies can be performed to obtain more accurate topological maps. However, the topological constructs are at a local image level than at a larger meta-level such as in this paper. In other words, [8] does not entertain notions of meta-level topological labels that go beyond an immediate lower-level topology restricted to the scene seen by the robot.

In this paper, we distinguish ourselves by portraying how higher level/meta level topological constructs that go beyond an immediate frame/scene and the relations that they enjoy amongst them percolate to a lower level pose-graph and elevate their metric relations. In fact, we recover close to ground truth floor plans from a highly disorganized map at the start. This is the essential contribution of the paper. In addition, the following constitute our contributions:

- 1) A deep convolutional network capable of learning warehouse topologies and ablation studies over the same.
- 2) A Siamese Neural Network based relational classifier which resolves topological element ambiguity and helps achieve an accurate pose graph purely based on Topological relations. Ablation studies are performed to signify the effectiveness of the classifier.
- 3) We showcase a backend SLAM framework that integrates loop closure relations from an intermediate level Manhattan Graph to the lowest level Pose Graph and elevate a disoriented unoptimized map to a structured optimized map which closely resembles the floor plan of the warehouse. Apart from the loop closure relations, the SLAM integrates other Manhattan relations to the pose graph. Ablation studies show the utility of both loop and Manhattan constraints as well as the superior performance of an incremental topological SLAM over a full batch topological SLAM. (Refer to Table III.)
- 4) We also show how the two-way exchange between the MG and PG further improves the accuracy of the PG . This two-way exchange between the various levels of representation is unique to this effort. Refer to the bottom two rows in Table III.

Through the above formulation, the paper essentially exploits the Manhattan properties present in indoor warehouse scenes to perform PG recoveries.

II. METHODOLOGY

Consider an unoptimized pose graph PG represented by its nodes as V_{pg} and edges as E_{pg} . The edges relation are of the following kinds:

*Denotes authors with equal contribution

This work was supported by Rapyuta Robotics. All authors associated with Robotics Research Center, KCIS, IIIT Hyderabad, India {ravi.kiran,mkrishna}@iiit.ac.in

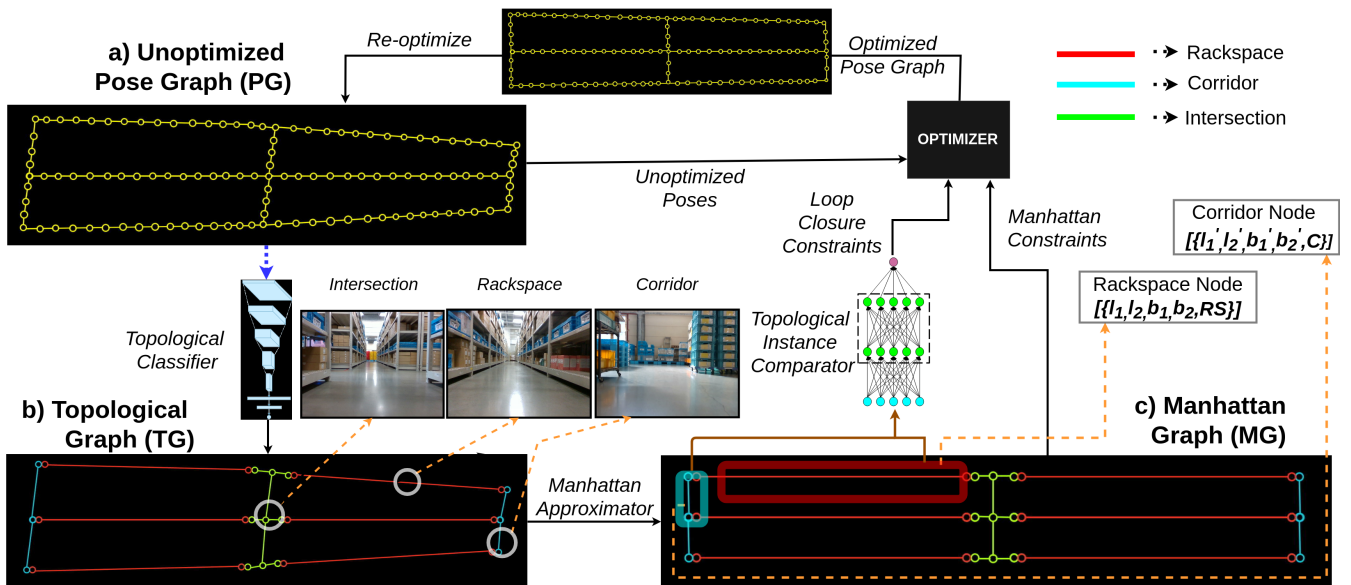


Fig. 1. Overall formulation presented with input as Pose-graph and CNN based classifier to classify regions. These classification labels are used to propose potentially similar regions in pose-graph using topological instance comparator which generates more constraints for pose graph. Additionally we generate topologically consistent graph called Manhattan graph which helps add more constraints in pose-graph eventually giving more relevant constraints to pose-graph to increase accuracy. The blue dotted arrow shows the start of the pipeline and then follows a feedback like structure.

- Odometry relation between successive nodes.
- Loop closure relation between a pair of nodes.
- Manhattan relation between a pair of nodes.

We obtain odometry relations from fused ICP and wheel odometry estimates which gives us the initial pose graph which is highly erroneous. We then leverage the topological and Manhattan level awareness to generate the loop closure and Manhattan relations and use them for pose graph optimization to recover accurate graphs. This whole process is divided into 3 sub-sections:

- 1) Topological categorization using a convolutional neural network classifier and its graph construction.
- 2) Constructing Manhattan Graph from the obtained Topological Graph and predicting loop closure constraints using Multi-Layer Perceptron.
- 3) Pose graph optimization using obtained Manhattan and loop closure constraints.

Each part of the pipeline is described in each sub-section below, followed by experiments and results which are explained in the next section.

A. Topological Categorization and Graph Construction

Every node $V_i \in V_{pg}$ is associated with a topological label $L(V_i)$ or L_i where $L_i \in L = \{rackspace, corridor, transitions\}$ for a warehouse scene. To obtain these topological labels from visual data, we train a Convolutional Neural Network (CNN) configured for classification. The training data consists of RGB images resized to 224×224 and paired with topological node labels. For our warehouse setting, the labels are Rackspace, Corridor, Intersection:

- Rackspace: Location on path between two rackspace

- Corridor: Location on the warehouse boundary path common to rackspace
- Intersection: A transition location on the path

Figure-1 entails examples of frames and their topological labels. We train a ResNet-18 [9] architecture pre-trained on ImageNet [10] with its final layer replaced by a 3-neuron fully connected layer, corresponding to the possible topological node labels. During training, we optimize the network to minimize cross-entropy loss. To account for class imbalance, we use class-weighted loss [11] with the following set of weights: Rackspace: 2.48, Corridor: 2.16, Intersection: 7.38. The CNN is fine-tuned for 356 epochs using Adam optimizer with a learning rate of 0.001 for the pre-trained ResNet-18 layers and a learning rate of 0.005 for the final layer weights. We stop training when the validation loss starts to increase. For training, we use 33,273 images from two warehouses with a mini-batch size of 8. To evaluate the trained network, we use 21,200 images. The results are presented in the next section.

After obtaining the inferred labels from the CNN, we group together the adjacent nodes that share the same label. Thus, a node in Topological Graph TG consists of two positions from the dense Pose Graph PG , i.e. the starting and ending positions of that topology.

B. Manhattan Graph Construction and Constraint Prediction using MLP

We now explain how the Topological Graph TG of the last section is converted to a Manhattan Graph, MG . We denote each node in the MG as a meta-node, $M_j \in MG$, where M_j corresponds to a collection C i.e. $V_i, V_{i+1}, \dots, V_{i+n}$ of PG nodes, such that we write $V_i \in C(M_j)$ and $L(M_j) = L(V_i)$

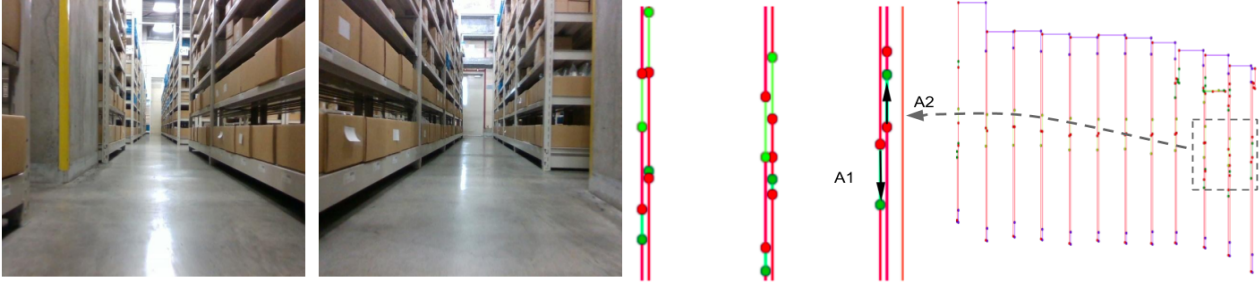


Fig. 2. We demonstrate the detection of similar nodes using MLP. Along the row we show an image pair along with its manhattan trajectory map and the location of the image pair on the manhattan map. The gray dotted box indicates the location of the overlapping intersection nodes which belong to the same topology in the global manhattan map. The gray dotted arrow points to the overlapping intersection nodes shown zoomed-in. The black arrows in the opposite direction depict the same region but viewed from opposite directions by the robot. Along the row the location of a particular 3-way intersection region from opposite views which belong to the same topology is shown. We denote the forward viewpoint of the 3-way intersection by A1. A2 denotes the same intersection from a backward viewpoint. We demonstrate detection of similar nodes which belong to the same topology at opposite viewpoints which is known to be a difficult task.

for every PG node in the collection set C . A new meta-node is formed when there is a change in the label.

The pose graph nodes, their corresponding topology labels shown in the color denoting the label, the collection of such nodes that constitute a meta node also shown in the same color in the MG are portrayed in figure 1.

The MG relies on two essential measurements for its construction.

- The length l of traversal or the length of topologies such as corridor or a rackspace.
- The angle ϕ made between two corridors/two rackspaces/rackspace and corridor via an intersection.

The length of the traversal is obtained by integrating fused odometry and ICP based transformations between two successive nodes of the Pose Graph that belong to the same meta node in the Manhattan Graph. The angle made as the robot moves from one topology (rackspace/corridor) to another (rackspace/corridor) via an intersection is estimated by fusing odometry and scan matching ICP measurements and integrating them over the traversal through the Intersection. This angle is binned to the closest multiple of $\pi/2$ as one of $\frac{-\pi}{2}, 0, \frac{\pi}{2}, \pi$. We use these sets of obtained lengths l and angles ϕ along with the category of the meta node M_j i.e. $L(M_j)$ as attributes as input to a Siamese-style MLP neural network in order to determine if any two nodes in MG are the same instance of a topological construct. In other words, the MLP determines if any two nodes in MG correspond to the same topological area of the workspace.

The training data for the MLP consists of what we have described as “meta-nodes” above. Each meta-node is a tuple consisting of $\{X_{start}, Y_{start}, X_{end}, Y_{end}\}$. The four values of the tuple denote the starting and ending displacement co-ordinate of a particular node with respect to a global origin (global origin is the point from where the robot starts moving in the warehouse). X_{start} and X_{end} denote the displacement co-ordinates in the x-direction. Y_{start} and Y_{end} denote the displacement co-ordinates in the y-direction. We create training data on the fly since we know the general structure of our warehouse and hence can create nodes

synthetically using random numbers with similar lengths. The architecture is a Siamese network [12] which consists of two hidden layers. We apply contrastive loss on the output obtained from the Siamese network to constrain semantically similar “meta-node” representations to lie closer to each other. During inference, the MLP compares two nodes of the Manhattan Graph and predicts if the nodes correspond to the same topological instance. We base our approach on two strong assumptions:

- Each node comprises of one contiguous region of one particular category.
- Each node has displacement only in one direction. (Along x or y).

The classification that results from the MLP is particularly powerful due to its ability to classify two topological instance to be the same even when viewed from opposing viewpoints. This is shown in Figure-2 where the same topology is viewed from opposite viewpoint and have little in common. Yet the MLP’s accurate classification of them to be the same instance becomes particularly useful for the Pose Graph optimization described in the next section.

The MLP’s non reliance on perceptual inputs also comes in handy for repetitive topologies. Warehouse scenes are often characterizes by repetitive structure and are prone to perceptual aliasing. The classification accuracy of the MLP is unaffected by such repetitiveness in the environment since it bypasses perceptual inputs. Yet the MLP does make use of perceptual inputs minimally in that it attempts to answer if the two nodes in the MG are the same instances only if the topological labels of the two nodes are predicted to be the same by the CNN.

C. Pose Graph Optimization

The Manhattan relation that exists between two nodes M_i, M_j and represented as $R(M_i, M_j) = \langle \Delta x_{ij}, \Delta y_{ij}, \Delta \theta_{ij} \rangle$ serves as a Manhattan constraint between the nodes corresponding to M_i, M_j in the pose graph (in a manner consistent with the edge relations given in posegraph libraries such as G2O [13], GT-SAM [14]).

$\Delta\theta_{ij}$ is typically 0° or 180° depending on whether the topology is being revisited with the same or opposing orientation.

The output of the MLP classifier is also used to invoke loop closure constraints. A pair of nodes classified to be the same topological construct by MLP corresponds to two sets of pose-graph nodes in the unoptimized graph belonging to the same area. Multiple loop closure relations are thus obtained between the pose-graph nodes of these two sets. Apart from these, there exist immediate Manhattan relations between two adjacent rackspaces or two adjacent corridors or a rackspace adjacent to a corridor mediated through an intersection. All such relations that exist in the Manhattan Graph as well as the loop closure relations percolate to the nodes in the PG as described further below.

In effect the optimizer solves for [15]:

$$\begin{aligned}
 X^* = \underset{X}{\operatorname{argmax}} P(X|U) &= \underset{X}{\operatorname{argmax}} \prod_i P(x_{i+1}|x_i, u_i) \\
 &\times \underbrace{\prod_{i \in C(M_i), j \in C(M_j)} P(x_j|x_i, c_{ij})}_{\text{Loop Closure Constraints}} \\
 &\times \underbrace{\prod_{i \in N(M_i), j \in N(M_j)} P(x_j|x_i, m_{ij})}_{\text{Manhattan Constraints}}
 \end{aligned}$$

where $P(X|U)$ is posterior probability of posegraph X over set of constraints U , x_i and u_i are i^{th} pose and controls of the robot. The loop closure relation c_{ij} between nodes i and j is obtained using ICP. There are in principle $n(C(M_i)) \times n(C(M_j))$ loop closure relations that are possible between topological constructs M_i, M_j where $C(M_i)$ is the collection set of Manhattan node M_i as described before and $n(P)$ is the cardinality of the set P . Whereas in practice we only sample a subset of such relations to constrain the graph.

Similarly, the graph is also constrained by Manhattan relations m_{ij} that are invoked between the pose-graph nodes that constitute the sets $N(M_i)$ and $N(M_j)$ where $N(M_i)$ and $N(M_j)$ represent the Pose Graph nodes within the neighbourhood of M_i and M_j .

Typically $N(M_j) \subseteq C(M_j)$. More formally, let S be the set that enumerates all loop closure pairs discovered by the MLP over a Manhattan Graph MG . i.e $S = \{(M_i, M_j), (M_j, M_k), \dots, (M_p, M_q)\}$, where each element of the set is a loop closure pair on the graph and $\{M_i, M_j, \dots, M_q\}$ are the nodes of the MG . Let i be an iterator iterating over the element of S , $S(i) = (M_p, M_q)$. Let LC be the set of all loop closure relations, c_{ij} obtained for every $S(i) \in S$ by sampling from the $n(C(M_i)) * n(C(M_j))$ number of loop closures possible for every $S(i) \in S$. Similarly, let M be the set of all Manhattan relation m_{ij} obtained for every $S(i) \in S$ from the neighbouring nodes in the unoptimized graph $N(M_i), N(M_j)$ for every $S(i) = (M_i, M_j) \in S$. Then

$$\begin{aligned}
 X^* = \underset{X}{\operatorname{argmax}} \prod_i P(x_{i+1}|x_i, u_i) \prod_{c_{ij} \in LC} P(x_j|x_i, c_{ij}) \\
 \prod_{m_{ij} \in M} P(x_j|x_i, m_{ij})
 \end{aligned}$$

III. EXPERIMENTATION AND RESULTS

A. Topological Categorization in a Real Warehouse Setting

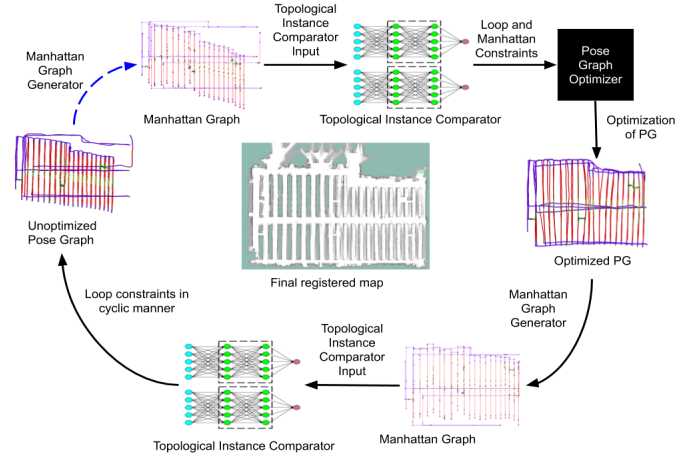


Fig. 3. We start with the unoptimized Pose Graph with drift (shown by dotted-blue arrow) and obtain its Manhattan Graph. The nodes of the Manhattan graph are then passed to the Topological Instance Comparator which acts like a Topological Instance comparator and gives out node pairs which belong to the same topology. This is then passed to the Pose Graph Optimizer which gives us optimized Pose Graph. We then obtain the Manhattan graph of the optimized Pose Graph. The nodes of this graph are passed to the Topological Instance comparator which gives us improved (more accurate) loop pairs. This complete pipeline is done multiple times in a cyclic manner till convergence. We finally get a registered map which is shown in the center.

The performance of the topological node classification CNN (Section II-A) can be viewed in Table I. For the combined dataset, the network is able to classify the rackspace and corridor with very low false positives and false negatives with precision and recall more than 94% each. However, it is relatively difficult to classify the third class i.e. intersection as there is not much semantic consistency as the robot moves from one topology to another, which is reflected in the fact that the recall value is quite low, about 78%. We explain how this inaccuracy affects the downstream modules in the Section III-D.

TABLE I

CNN CLASSIFICATION RESULTS.

Warehouse dataset	Accuracy	Metrics for Combined Data (1&2)		
		Category	Precision	Recall
1&2	93.75	Rackspace	94.2	96.3
1	95.15	Corridor	96.3	96.4
2	89.06	Intersection	85.6	78.1

B. Efficacy of Loop Closure Constraint Prediction using MLP

TABLE II
MLP RESULTS

Network Type	Warehouse-1	Warehouse-2
Accuracy	71.2	67.7

We showcase our pipeline on two different warehouses. There were two experiments performed. First, we sample our training data according to the layout and length constraints of warehouse-1 and use the data-points of warehouse-1 as the lone testing data. In our second experiment, we train our MLP specifically according to the layout and length constraints of warehouse-2.

The detection of nodes belonging to the same topology was observed to be accurate at the initial phase of the trajectory. The latter part of the trajectory was not accurate and had drift due to which the detection of node-pairs was observed to be inaccurate (Unoptimized Pose Graph shown in Figure-3). We were able to improve the accuracy of the MLP and were able to generate accurate loop pairs by performing optimization on the Pose Graph in a cyclic fashion as shown in Figure-3.

We performed the experiments on both warehouses. The accuracy is calculated by checking for the percentage of the true node pairs. An accuracy of 71.2% and 67.7% was observed for the first and the second warehouse respectively.

C. Pose graph optimization Results

The ablation study on the type of constraints have been done in five stages. The robustness of map recovery increases with each stage which reflects in Absolute Trajectory Error in Table III.

1) Stages of Map Recovery:

- (i) *Manhattan constraints:* Only manhattan constraints are used to optimize pose graph, PG. Constraints are extracted from manhattan graph, MG, between nodes proposed by MLP to be similar.
- (ii) *Loop Closure and Manhattan constraints:* Apart from Manhattan constraints, Loop Closure constraints as explained in section II-C are also used to constrain the PG.
- (iii) *Dense Proposals from MLP:* We consider nodes that have been classified to belong to the same instance with low confidence along with those classified to be the same with high confidence. This increases the number of constraints improving the optimization performance. The wrongly detected loops are filtered based on the loop closure (ICP) residual cost and do not make it to the optimization.
- (iv) *Dense Proposals by MLP in Feedback Loop:* A feedback loop is invoked on the optimized PG from previous stage. A new MG is computed on the optimized PG, this manhattan graph, MG, is feeded to MLP and sets of constraints are generated in a cyclic manner.

This feedback mechanism leads to MLP performance improvement as shown in Table IV and also helps in achieving very low Absolute Trajectory Error, ATE of 1.82 meters on four different maps from 11.57 meters in unoptimized map. This corresponds to the fourth of the contribution mentioned in the Section I.

- (v) *Incremental formulation:* Performing the feedback strategy from the previous stage in an incremental formulation in ISAM [14] helps us to achieve the lowest ATE of 1.45 meters in our system. This confirms the robustness of our system to recover from highly unoptimized trajectories.

2) *Qualitative Results:* We evaluate our system in two challenging real warehouse settings. The warehouse dimensions are $30m \times 50m$ and contains 21 rackspaces with intermediate corridors and intersections. All experiments start with highly deformed trajectories. In all the cases, we were able to recover trajectories close to the groundtruth. Note that in our case, the ground-truth trajectory is the optimized map from the cartographer that has been confirmed with warehouse floor plan by our collaborators. These results are shown in Figure 5. The top row shows highly distorted pose graph trajectories while the middle row showcases the results of our optimization framework. The last row depicts the ground truth trajectories. The overall pipeline gets best illustrated with Figure 3.

D. Robustness Analysis

We analyze the performance of the topological SLAM due to errors in topological classification due to the CNN and due to failure to detect loops by the MLP. Errors in topology classification manifest as loop detection in the MG. Therefore, the analysis is one of the robustness due to wrong loop detection wherein both false positive and false negative cases are considered. The robustness to the pose graph optimization stems due from the following features:

- 1) Residuals in the ICP estimated loop closure end up serving as priors to the element of dynamically scaled covariance matrix [7], which serves as a robust kernel providing for backend topology recovery even when the number of wrong loop closures increase.
- 2) An optimized PG feeds back to the MG and alleviates its error. The improved MG improve the loop detection performance of MLP, which percolate to the PG nodes and further improve its accuracy. Overtime this iterative exchange of information between the various representations improves the robustness of the PG backend.

To analyse the performance of our robust kernel exclusively in presence of the outliers, we synthetically introduced false positive and false negative loop closure pairs in the constraints for PG. In Figure 4 X-axis represents percentage of loop closure pairs in the data-set having equal amount of false positive and false negative pairs. Y-axis represents ATE of TG with respect to the ground truth. The Figure 4 depicts the performance of our framework due to errors occurred in topology classification and loop detection.

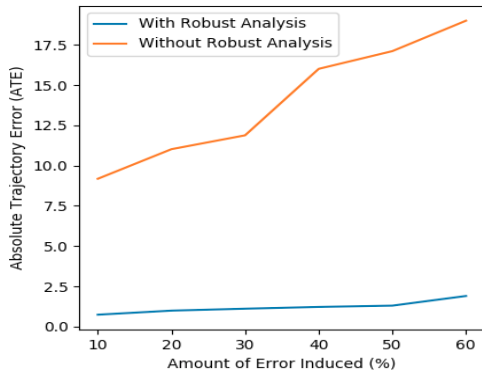


Fig. 4. Effect of Robust pose-graph optimization with DCS

From the analysis of results in Figure 4 it is evident that gradual increase in outliers can be tolerated by Robust kernel with DCS [7] as compared with non robust optimization techniques.

TABLE III
ABSOLUTE TRAJECTORY ERROR(ATE) [16] FOR VARIOUS POSE-GRAPHS WITH RESPECT TO GROUND-TRUTH TRAJECTORIES. LC STANDS FOR 'LOOP CLOSURE CONSTRAINTS'

Method Type	W-2.1	W-2.2	W-1.1	W-1.2	Avg
	ATE	ATE	ATE	ATE	ATE
Unoptimized	4.7	7.5	16.3	17.8	11.57
MLP Manhattan (G2O)	3.42	2.85	4.5	7.4	4.54
MLP Manhattan + LC (G2O)	3.09	2.7	3.9	1.67	2.84
Dense MLP Manhattan + LC (G2O)	1.98	1.96	2.75	1.65	2.08
Dense MLP Manhattan + LC (In Feedback Loop) (G2O)	1.67	1.8	2.21	1.6	1.82
Dense MLP Manhattan + LC (In Feedback Loop) (iSAM)	1.6	0.98	1.02	2.2	1.45

TABLE IV
EFFECT OF FEEDBACK MECHANISM ON MLP PERFORMANCE

	True Positive	False Positive	Accuracy
MLP	119	81	59.5
MLP in Feedback Loop	133	55	70.7

IV. CONCLUSION AND FUTURE WORK

This paper shows how higher level abstractions of an indoor workspace such as real warehouses can be used to effectively improve lower level backend modules of localization and mapping. Specifically we show how higher and intermediate level abstractions in the form of Topological Graph and Manhattan Graph can recover from backend pose graph optimization failures. Further by constant information exchange between the various levels of map abstractions we improve quantitatively the ATE by more than 87.4% starting

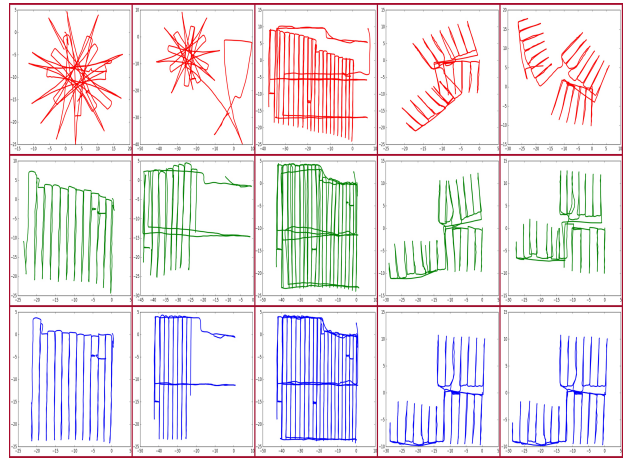


Fig. 5. Top row shows unoptimized trajectories, middle row shows trajectories recovered using our pipeline and last row shows ground truth trajectories. Length in metres is shown along X and Y axes.

from very distorted pose graphs. We further show the method is robust to failures in the higher level representations such, which occurs when the Deep CNN architecture wrongly classifies a topological construct or when the Siamese style classifier wrongly detects or fails to detect loops in the Manhattan graph. The results shown are on two different real warehouse scenes over an area of around $30m \times 50m$, filled with many repetitive topologies in the form of corridor areas and rackspaces. Future results are intended to be shown on a variety of indoor topologies and office spaces such as for example those found in the Gibson environment [17].

REFERENCES

- [1] Emilio Garcia-Fidalgo and Alberto Ortiz. Vision-based topological mapping and localization methods: A survey. *Robotics and Autonomous Systems*, 64:1–20, 2015.
- [2] Iwan Ulrich and Illah Nourbakhsh. Appearance-based place recognition for topological localization. In *Proceedings 2000 ICRA. Millennium Conference. IEEE International Conference on Robotics and Automation. Symposia Proceedings (Cat. No. 00CH37065)*, volume 2, pages 1023–1029. Ieee, 2000.
- [3] Niko Sünderhauf and Peter Protzel. Switchable constraints for robust pose graph slam. In *2012 IEEE/RSJ International Conference on Intelligent Robots and Systems*, pages 1879–1884. IEEE, 2012.
- [4] Andrzej Pronobis, Barbara Caputo, Patric Jensfelt, and Henrik I Christensen. A discriminative approach to robust visual place recognition. In *2006 IEEE/RSJ International Conference on Intelligent Robots and Systems*, pages 3829–3836. IEEE, 2006.
- [5] Ananth Ranganathan and Frank Dellaert. A rao-blackwellized particle filter for topological mapping. In *Proceedings 2006 IEEE International Conference on Robotics and Automation, 2006. ICRA 2006.*, pages 810–817. IEEE, 2006.
- [6] Jana Kosecka, Liang Zhou, Philip Barber, and Zoran Duric. Qualitative image based localization in indoors environments. In *2003 IEEE Computer Society Conference on Computer Vision and Pattern Recognition, 2003. Proceedings.*, volume 2, pages II–II. IEEE, 2003.
- [7] Pratik Agarwal, Gian Diego Tipaldi, Luciano Spinello, Cyrill Stachniss, and Wolfram Burgard. Robust map optimization using dynamic covariance scaling. In *2013 IEEE International Conference on Robotics and Automation*, pages 62–69. Citeseer, 2013.
- [8] Ananth Ranganathan, Emanuele Menegatti, and Frank Dellaert. Bayesian inference in the space of topological maps. *IEEE Transactions on Robotics*, 22(1):92–107, 2006.
- [9] Kaiming He, Xiangyu Zhang, Shaoqing Ren, and Jian Sun. Deep residual learning for image recognition. In *Proceedings of the IEEE conference on computer vision and pattern recognition*, pages 770–778, 2016.
- [10] J. Deng, W. Dong, R. Socher, L.-J. Li, K. Li, and L. Fei-Fei. ImageNet: A Large-Scale Hierarchical Image Database. In *CVPR09*, 2009.
- [11] Justin M Johnson and Taghi M Khoshgoftaar. Survey on deep learning with class imbalance. *Journal of Big Data*, 6(1):27, 2019.
- [12] Jane Bromley, Isabelle Guyon, Yann LeCun, Eduard Säckinger, and Roopak Shah. Signature verification using a” siamese” time delay neural network. In *Advances in neural information processing systems*, pages 737–744, 1994.
- [13] Rainer Kümmeler, Giorgio Grisetti, Hauke Strasdat, Kurt Konolige, and Wolfram Burgard. g 2 o: A general framework for graph optimization. In *2011 IEEE International Conference on Robotics and Automation*, pages 3607–3613. IEEE, 2011.
- [14] Michael Kaess, Ananth Ranganathan, and Frank Dellaert. isam: Incremental smoothing and mapping. *IEEE Transactions on Robotics*, 24(6):1365–1378, 2008.
- [15] Niko Sünderhauf and Peter Protzel. Brief-gist-closing the loop by simple means. In *2011 IEEE/RSJ International Conference on Intelligent Robots and Systems*, pages 1234–1241. IEEE, 2011.
- [16] Jürgen Sturm, Nikolas Engelhard, Felix Endres, Wolfram Burgard, and Daniel Cremers. A benchmark for the evaluation of rgb-d slam systems. In *2012 IEEE/RSJ International Conference on Intelligent Robots and Systems*, pages 573–580. IEEE, 2012.
- [17] Fei Xia, Amir R. Zamir, Zhi-Yang He, Alexander Sax, Jitendra Malik, and Silvio Savarese. Gibson env: real-world perception for embodied agents. In *Computer Vision and Pattern Recognition (CVPR), 2018 IEEE Conference on*. IEEE, 2018.

V. APPENDIX

A. Method of Manhattan Graph Generation and Input Data to MLP

We first start with unoptimized trajectory (figure 6) and then label the trajectory with topological categories obtained from our place recognition network. Then a sparse representation of this dense trajectory is obtained by representing a topology with its starting and ending points along with its label. If a topology is bent at 90, 180 or 270 degrees, then we split the topology into two parts at the bent point. In this way each topological region is represented by lines characterized by its starting and ending positions along with its label. Then due to the prior that warehouses are manhattan in nature, we incorporate this prior in the sparse representation and the angles between two topological regions are binned to the nearest manhattan angle, i.e. 90, 180 or 270 degrees. Thus the input to MLP is starting and ending X and Y coordinates of manhattan graph along with topological label.

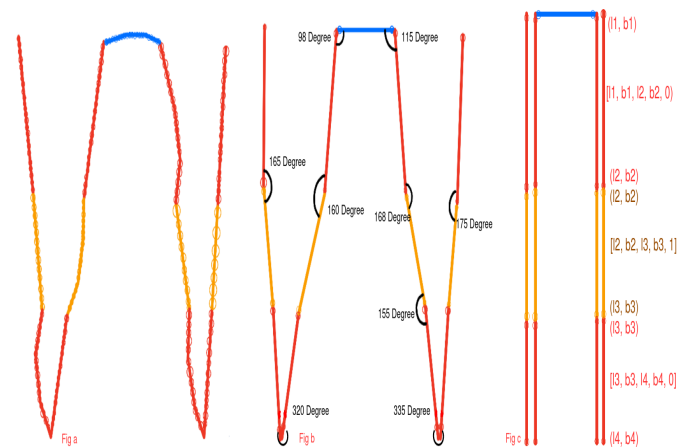


Fig. 6. Fig. a shows unoptimized trajectory with dense poses along with topological label. Fig. b shows sparse sparse trajectory obtained by approximating each topological region with its starting and ending position. Notice that irregular robot trajectory inside some topological regions are also approximated to be straight line. Fig. c shows manhattan graph generated by binning angles between two nodes to their nearest multiple of 90 degree. The input vector to the MLP is shown in middle of each node, which consists of its starting and ending coordinates, along with topological label.

B. Comparison of Our Topological Slam Pipeline with Traditional Slam Method, RTABMAP

We compare our topological slam pipeline with state of the art SLAM system RTABMAP, it is a highly modular library with integration of various sensors fusion like monocular camera, stereo camera, Lidar, IMU, wheel odometry etc. In the first experiment we ran RTABMAP with all the predefined parameters for frontend, loop closure and backend. In the second experiment, we ran RTABMAP, just as a odometry pipeline by disabling loop closure and global pose optimization (shown in the next section). In both the cases, our pipeline is able to surpass the trajectory obtained from RTABMAP. In both the experiments, the input trajectory to our pipeline is obtained from the output of RTABMAP.

1) *Experiment 1: RTABMAP with Loop closure on:* In the first experiment, there are many false loop closures detected by the RTABMAP at the end of each corridor, so they are merged into the same corridor, while because of the incorporation of manhattan constraints in our pipeline, ends of each corridor is treated as separate regions. Figure 7 qualitatively shows the superior performance of our pipeline with RTABMAP. The input to our pipeline is the final optimized trajectory obtained from RTABMAP, which shows that we can use Topological Slam formulation to improve RTABMAP.

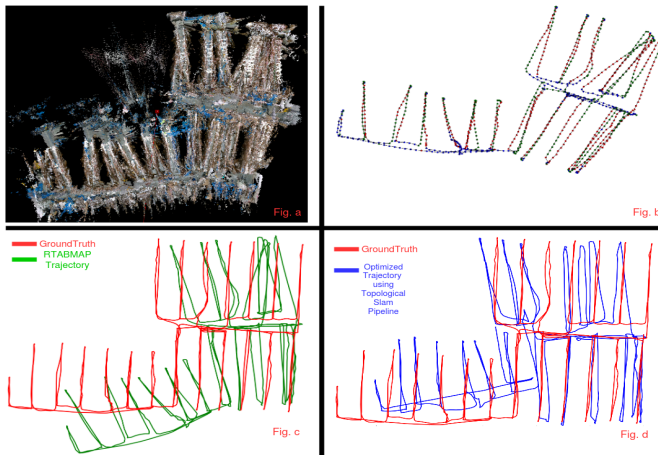


Fig. 7. Fig. a shows registered map generated by RTABMAP Slam. Fig. b shows RTABMAP trajectory with topological labels. Fig. c compares the RTABMAP trajectory with groundtruth trajectory. Fig. d compares trajectory generated using our topological SLAM pipeline with groundtruth

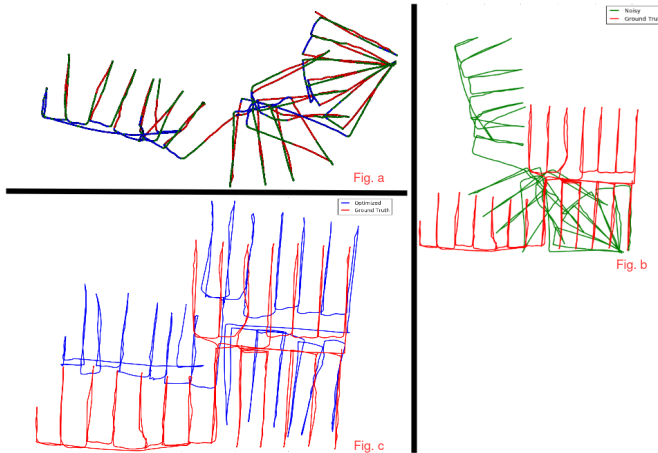


Fig. 8. Fig. a shows trajectory obtained using RTABMAP with loop closure turn off. Wheel odometry is used as odometry source. Fig. b compares RTABMAP trajectory with groundtruth. Fig. c compares trajectory obtained using Topological Slam pipeline with groundtruth.

2) *Experiment 2: RTABMAP with Loop closure off:* In the second experiment, due to lack of loop of closure module, RTABMAP trajectory is drifting at the turning points of the robots. While with manhattan and loop constraints

from MLP, our trajectory is quite closed to ground-truth. The input to our pipeline is again trajectory obtained using RTABMAP, which shows that our pipeline can be used to extend RTABMAP performance in Manhattan like environments. Figure 8 qualitatively compares RTABMAP with our pipeline without Loop closure and Global pose graph optimization.